GROUP-BASED TRUNCATED L_{1-2} MODEL FOR IMAGE INPAINTING

Tian-Hui Ma[⋆] *Yifei Lou*[†] *Ting-Zhu Huang*[⋆] *Xi-Le Zhao*[⋆]

[⋆] School of Mathematical Sciences/Research Center for Image and Vision Computing, University of Electronic Science and Technology of China, Chengdu 611731, China.
[†] Department of Mathematical Sciences, University of Texas at Dallas, Dallas, TX 75080, USA.

ABSTRACT

We propose a novel image inpainting model that can effectively estimate missing pixels in an observed image. The latent image is characterized by a group-based low-rank prior, which assumes that a group of vectorized similar image patches can be well approximated by a low-rank matrix. We enforce the low-rankness of each group by penalizing a truncated difference of the l_1 and the l_2 norms of its singular values, which achieves a close approximation to the matrix rank. We apply a difference of convex algorithm (DCA) to solve the proposed model efficiently. Our method is validated on filling missing blocks and randomly missing pixels, with superior performance over the state-of-the-art.

Index Terms— Difference of convex functions algorithm, image inpainting, l_{1-2} minimization, low-rank matrix approximation, nonlocal self-similarity

1. INTRODUCTION

Image inpainting [1] aims to complete the missing pixels in an observed image so that the resulting image is natural to human eyes. It is a typical inverse problem with infinitely many solutions. To obtain meaningful results, all methods rely on some prior knowledge about the latent image.

Existing inpainting methods can be roughly categorized into three classes: diffusion-based methods, sparsity-based methods, and exemplar-based methods. Diffusion-based methods [1, 2] introduce piecewise smoothness image priors to diffuse local image structures from the known region to the missing region. They preserve well smooth objects and strong edges but smear out repetitive textures. Sparsity-based methods [3, 4] assume the sparsity of natural images under transform domains or over-complete dictionaries, and the missing structures are estimated by promoting their sparse representations. These methods perform well on filling small regions, but tend to introduce blurry effects when dealing with large missing areas. Exemplar-based methods [5, 6] exploit the redundancy of similar image features at distant regions, also known as nonlocal self-similarity (NNS), and the missing region is completed by copying similar patches selected from the known part of the image. These methods are particularly suitable for large region inpainting and object removal. We refer the reader to [7] for a comprehensive overview of image inpainting methods.

Recently, image priors combining sparsity and NNS have achieved great success in image inpainting [8, 9]. The basic idea is that a data array consisting of similar image patches, referred to as a group, exhibits strong sparsity under a certain transform [9]. Particularly, the group-based low-rank prior [8] assumes that each group/matrix with vectorized similar image patches as its columns has low rank, which can be considered as being sparse after singular value decomposition (SVD). By enforcing each group to be sparse/low-rank, these methods benefit from a sparse and redundant image representation in terms of group, characterizing both the sparsity and NNS of natural images in a unified framework.

An appropriate sparsity measure plays a central role in sparse representation. Recently, Esser et al. [10] proposed a nonconvex l_{1-2} metric for sparse promotion, defined as $\|\mathbf{x}\|_{1-2} := \|\mathbf{x}\|_1 - \|\mathbf{x}\|_2$. The l_{1-2} metric has shown to recover sparse vectors better than the convex l_1 norm in various applications [11, 12, 13, 14, 15]. However, we showed in [16] that l_{1-2} may not approximate the vector sparsity well when the number of large entries (in magnitude) increases; and we proposed a truncated l_{1-2} metric, denoted as $l_{t,1-2}$, to overcome this drawback. The main idea is to discard large magnitudes in penalization, thus achieving a close approximation to the vector sparsity and the matrix rank (sparsity of singular values). Particularly, the matrix version of $l_{t,1-2}$ is defined as a truncated difference of l_1 and l_2 norms of singular values,

$$\|\mathbf{X}\|_{t,*-F} := \sum\nolimits_{i>t} \sigma_i(\mathbf{X}) - \sqrt{\sum\nolimits_{i>t} \sigma_i^2(\mathbf{X})}, \quad (1)$$

where $\sigma_i(\mathbf{X})$ is the ith largest singular value of $\mathbf{X}$ and t is the number of truncated singular values. We demonstrated in [16] that $l_{t,1-2}$ is superior over many nonconvex metrics including l_{1-2} in recovering sparse vectors and low rank matrices.

Please address correspondences to: nkmth0307@126.com.

⋆ These authors' work was supported by 973 Program (Grant No. 2013CB329404), NSFC (Grant No. 61370147, 61402082), the Fundamental Research Funds for the Central Universities (Grant No. ZYGX2016J132).

† This author's work was supported by NSF grant DMS-1522786.

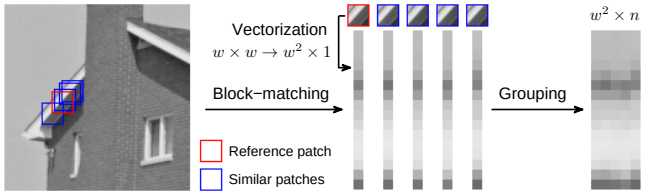

Fig. 1. Illustration of constructing groups by block-matching (BM) [19]. For each $w \times w$ reference patch from an $n_1 \times n_2$ image, we use block-matching [19] to search its $n-1$ best matched patches in terms of Euclidean distance, and then vectorize and combine those patches to form a group of size $w^2 \times n$. Mathematically, this process can be expressed as a linear operator $R : \mathbb{R}^{n_1 \times n_2} \to \mathbb{R}^{w^2 \times n}$.

We propose in this paper to incorporate $l_{t,1-2}$ into a group-based low-rank model for image inpainting. In particular, we aim at minimizing

$$\begin{aligned} \min_{\mathbf{X}} \ & F(\mathbf{X}) := \textstyle\sum_{k=1}^{s} \|R_k(\mathbf{X})\|_{t_k,*-F}, \\ \text{s.t.} \ & x_{i,j} = u_{i,j}, (i,j) \in \Omega, \\ & x_{i,j} \in [0,1], (i,j) \in \Omega^c, \end{aligned} \tag{2}$$

where $\mathbf{U}$ with pixels $\{u_{i,j}\}$ is the observed image, Ω is the known region, R_k is the extraction operator for the kth group (see Fig. 1 for an illustration), t_k is the number of truncated singular values for the kth group, and s is the total number of groups. The proposed model is able to achieve a close approximation of the rank of each group, combining the advantages of the group-based low-rank prior in image characterization and the $l_{t,1-2}$ metric in low-rankness promoting. We apply the difference of convex functions algorithm (DCA) [17] to decompose the proposed nonconvex problem into a series of convex subproblems, which can be efficiently solved by alternating direction method of multipliers (ADMM) [18]. Experimental results show the superior performance of our method over several state-of-the-art competitors.

The rest of the paper is organized as follows. Section 2 elaborates on our numerical scheme. Section 3 is devoted to experimental results. Finally, Section 4 concludes the paper.

2. NUMERICAL ALGORITHM

We use the DCA [17] to solve the proposed model, which is a descent algorithm for minimizing an objective with structure $G(\mathbf{X}) - H(\mathbf{X})$, where G and H are proper, lower semicontinuous, and strongly convex functions. The DCA starts from an initial point $\mathbf{X}^{(1)}$ and iterates as follows:

$$\begin{cases} \mathbf{Y}^{(l)} \in \partial H(\mathbf{X}^{(l)}), \\ \mathbf{X}^{(l+1)} = \arg\min_{\mathbf{X}} G(\mathbf{X}) - \langle \mathbf{Y}^{(l)}, \mathbf{X} \rangle, \end{cases} \tag{3}$$

where $\mathbf{Y}^{(l)} \in \partial H(\mathbf{X}^{(l)})$ means that $\mathbf{Y}^{(l)}$ is a subgradient of $H(\mathbf{X})$ at $\mathbf{X}^{(l)}$. Theoretical analyses of the DCA as well as the convergence to a critical point can be found in [17].

To make the DCA applicable, we rewrite $\|\mathbf{X}\|_{t,*-F} = \|\mathbf{X}\|_* - \|\mathbf{X}\|_{t,*+F}$, where

$$\|\mathbf{X}\|_{t,*+F} := \sum_{i=1}^{t} \sigma_i(\mathbf{X}) + \sqrt{\sum_{i>t} \sigma_i^2(\mathbf{X})}.$$

It has been established in [16] that $\|\mathbf{X}\|_{t,*+F}$ is a unitarily invariant norm. Then we rewrite (2) as $G(\mathbf{X}) - H(\mathbf{X})$, where

$$\begin{aligned} G(\mathbf{X}) &:= \textstyle\sum_{k=1}^{s} (\|R_k(\mathbf{X})\|_* + c\|R_k(\mathbf{X})\|_F^2) \\ &\quad + \textstyle\sum_{(i,j)\in\Omega} \delta_{\{u_{i,j}\}}(x_{i,j}) + \sum_{(i,j)\in\Omega^c} \delta_{[0,1]}(x_{i,j}), \\ H(\mathbf{X}) &:= \textstyle\sum_{k=1}^{s} (\|R_k(\mathbf{X})\|_{t_k,*+F} + c\|R_k(\mathbf{X})\|_F^2), \end{aligned} \tag{4}$$

where c is a positive constant to ensure strong convexity of G and H, and $\delta_\Lambda(\cdot)$ denotes the indicator function of a nonempty set Λ, i.e., $\delta_\Lambda(x) = 0$ if $x \in \Lambda$ and $\delta_\Lambda(x) = \infty$ if $x \notin \Lambda$. It is straightforward that (4) fits the DCA's framework.

A closed-form solution of $\mathbf{Y}^{(l)}$ in (3) is given by

$$\mathbf{Y}^{(l)} = \sum_{k=1}^{s} R_k^T(\mathbf{D}_k + 2cR_k(\mathbf{X}^{(l)})), \tag{5}$$

where $R_k^T : \mathbb{R}^{w^2 \times n} \to \mathbb{R}^{n_1 \times n_2}$ denotes the adjoint operator of R_k and $\mathbf{D}_k \in \partial\|R_k(\mathbf{X}^{(l)})\|_{t_k,*+F}$. To compute $\mathbf{D}_k$, we consider an economy SVD of $R_k(\mathbf{X}^{(l)})$ as $\mathbf{W}\mathrm{diag}(\boldsymbol{\sigma})\mathbf{V}^T$, where $\boldsymbol{\sigma}$ is a vector containing the positive singular values of $R_k(\mathbf{X}^{(l)})$. Define $\mathbf{d}$ by

$$d_i := \begin{cases} 1 & \text{if} \quad i \le t_k, \\ \sigma_i / \sqrt{\sum_{j>t_k} \sigma_j^2} & \text{if} \quad i > t_k, \end{cases}$$

and $\mathbf{D}_k := \mathbf{W}\mathrm{diag}(\mathbf{d})\mathbf{V}^T$. The fact that $\mathbf{D}_k \in \partial\|R_k(\mathbf{X}^{(l)})\|_{t_k,*+F}$ is proved in [16].

We use ADMM [18] to solve the convex $\mathbf{X}$-subproblem in (3). In particular, we introduce auxiliary variables $\{\mathbf{P}_k\}_{k=1}^s$ and rewrite the $\mathbf{X}$-subproblem as

$$\begin{aligned} \min_{\mathbf{X},\{\mathbf{P}_k\}_{k=1}^s} & \textstyle\sum_{k=1}^{s} (\|\mathbf{P}_k\|_* + c\|R_k(\mathbf{X})\|_F^2) - \langle \mathbf{Y}, \mathbf{X} \rangle, \\ & + \textstyle\sum_{(i,j)\in\Omega} \delta_{\{u_{i,j}\}}(x_{i,j}) + \sum_{(i,j)\in\Omega^c} \delta_{[0,1]}(x_{i,j}), \\ \text{s.t.} \quad & \mathbf{P}_k = R_k(\mathbf{X}), \text{ for } k = 1, \ldots, s, \end{aligned} \tag{6}$$

where the superscript (l) on $\mathbf{Y}$ is omitted without confusion. Denoting the objective of (6) as $E(\mathbf{X}, \{\mathbf{P}_k\}_{k=1}^s)$, we express the augmented Lagrangian function of (6) as

$$\begin{aligned} L(\mathbf{X}, \{\mathbf{P}_k\}_{k=1}^s, \{\mathbf{A}_k\}_{k=1}^s) &= E(\mathbf{X}, \{\mathbf{P}_k\}_{k=1}^s) \\ &\quad + \beta/2 \textstyle\sum_{k=1}^{s} \|\mathbf{P}_k - R_k(\mathbf{X}) + \mathbf{A}_k\|_F^2, \end{aligned} \tag{7}$$

where $\{\mathbf{A}_k\}_{k=1}^s$ denotes Lagrangian multipliers and $\beta > 0$ is a penalty parameter. Starting from initial points $\mathbf{X}^{(1)}$ and $\{\mathbf{A}_k^{(1)}\}_{k=1}^s$, ADMM proceeds as

$$\begin{cases} \{\mathbf{P}_k^{(m+1)}\}_{k=1}^s = \arg\min\limits_{\{\mathbf{P}_k\}_{k=1}^s} L(\mathbf{X}^{(m)}, \{\mathbf{P}_k\}_{k=1}^s, \{\mathbf{A}_k^{(m)}\}_{k=1}^s), \\ \mathbf{X}^{(m+1)} = \arg\min\limits_{\mathbf{X}} L(\mathbf{X}, \{\mathbf{P}_k^{(m+1)}\}_{k=1}^s, \{\mathbf{A}_k^{(m)}\}_{k=1}^s), \\ \{\mathbf{A}_k^{(m+1)}\}_{k=1}^s = \{\mathbf{A}_k^{(m)} + \mathbf{P}_k^{(m+1)} - R_k(\mathbf{X}^{(m+1)})\}_{k=1}^s. \end{cases} \tag{8}$$

Note that the minimizations with respect to $\mathbf{P}_k$ and $\mathbf{X}$ have closed-form solutions:

$$\mathbf{P}_k^{(m+1)} = \mathrm{SVT}(R_k(\mathbf{X}^{(m)}) - \mathbf{A}_k^{(m)}, 1/\beta), \tag{9}$$

$$x_{i,j}^{(m+1)} = \begin{cases} \iota_{[0,1]}((\bar{R}(\bar{\mathbf{X}}))_{i,j}), & (i,j) \in \Omega^c, \\ u_{i,j}, & (i,j) \in \Omega, \end{cases} \tag{10}$$

where $\mathrm{SVT}(\cdot,\cdot)$ denotes the singular value thresholding (SVT) formula [20], $\iota_\Lambda(\cdot)$ denotes the projection onto a nonempty set Λ, $\bar{R} := (\sum_{k=1}^s R_k^T R_k)^{-1}$, and

$$\bar{\mathbf{X}} := \left(\beta \sum\nolimits_{k=1}^s R_k^T(\mathbf{P}_k^{(m+1)} + \mathbf{A}_k^{(m)}) + \mathbf{Y}\right)/(\beta + 2c).$$

We remark that the operator $\bar{R}$ is an entry-wise division such that $(\bar{R}(\cdot))_{i,j} = \cdot_{i,j}/q_{i,j}$, where $q_{i,j}$ counts the number of times that $x_{i,j}$ occurs in all the groups $\{R_k(\mathbf{X})\}_{k=1}^s$. The convergence of ADMM for a convex problem is guaranteed; see [21] for more details.

We propose an adaptive strategy to select t_k for each $R_k(\mathbf{X})$. Let $\boldsymbol{\sigma}$ be a vector of all the singular values of $R_k(\mathbf{X})$ in a descending order. Given parameters $0 \le \theta, \eta \le 1$, t_k is selected as the maximal t satisfying

$$\sum\nolimits_{i=2}^t \sigma_i \le \theta \sum\nolimits_{i\ge 2} \sigma_i \quad \text{and} \quad \sigma_t \ge \eta \mathrm{mean}(\boldsymbol{\sigma}), \tag{11}$$

where $\mathrm{mean}(\cdot)$ denotes the vector mean. The first constraint in (11) ensures that a large portion of the group energy is truncated so that our prior achieves a close approximation to the matrix rank. Here the leading singular value σ_1 is always truncated since it is much larger than the rest ones ($\sigma_1 > 10\sigma_2$ in practice). The second requirement in (11) avoids truncating too many small singular values, which makes our algorithm unstable.

The pseudo-code of the overall algorithm is summarized in Algorithm 1. Here are some implementation details. We refine the grouping results at certain iterations, indicated in the finite set L_{BM}. After each update of grouping, we reinitialize each t_k with a small value and increase it gradually according to a set of increasing thresholdings, given in the vector $\boldsymbol{\theta}$. We remark that both $\{R_k\}_{k=1}^s$ and $\{t_k\}_{k=1}^s$ are fixed after finite number of iterations and hence convergence analysis of the DCA is applicable for our algorithm. The main computation of our algorithm lies in computing the SVDs in (9), whose complexity is $\mathcal{O}(s\min(w^4 n, w^2 n^2)$. Since the growth rate of s is $\mathcal{O}(n_1 n_2)$, one can deduce that the total complexity depends linearly on the image size, as all parameters are fixed.

Algorithm 1. The DCA for solving (2).

Input: $\mathbf{U}$, Ω, c, β, $\boldsymbol{\theta}$, η, L_{BM}, $l_{\max}$, $m_{\max}$, ϵ_{in}, and ϵ_{out}.

Initialization: Estimate an initial image $\mathbf{X}^{(1)}$ using cubic interpolation. Set $\mathbf{A}_k^{(1)} := \mathbf{0}$ for $k = 1, \ldots, s$, and $i := 1$.

Outer loop: For $l = 1, \ldots, l_{\max}$ **do**

1. If $l \in L_{\mathrm{BM}}$, perform grouping on $\mathbf{X}^{(l)}$ to get $\{R_k\}_{k=1}^s$ and set $i := 1$.
2. If $i \le \mathrm{length}(\boldsymbol{\theta})$, compute $\{t_k\}_{k=1}^s$ from (11) using (θ_i, η) and set $i := i + 1$.
3. Compute $\mathbf{Y}^{(l)}$ from (5) using $\{t_k\}_{k=1}^s$.
4. Set $\mathbf{X}^{(l+1,1)} := \mathbf{X}^{(l)}$ and $\{\mathbf{A}_k^{(l+1,1)}\}_{k=1}^s := \{\mathbf{A}_k^{(l)}\}_{k=1}^s$.

   Inner loop: For $m = 1, \ldots, m_{\max}$ **do**

   a. Compute $\{\mathbf{P}_k^{(l+1,m+1)}\}_{k=1}^s$ by (9).

   b. Compute $\mathbf{X}^{(l+1,m+1)}$ by (10).

   c. Update $\{\mathbf{A}_k^{(l+1,m+1)}\}_{k=1}^s$ by (8).

   d. If $\frac{\|\mathbf{X}^{(l+1,m+1)} - \mathbf{X}^{(l+1,m)}\|_F}{\|\mathbf{X}^{(l+1,m)}\|_F} \le \epsilon_{\mathrm{in}}$, set $m := m + 1$ and **Break** inner loop.

   End Inner loop and output $\mathbf{X}^{(l+1)} := \mathbf{X}^{(l+1,m)}$ and $\{\mathbf{A}_k^{(l+1)}\}_{k=1}^s := \{\mathbf{A}_k^{(l+1,m)}\}_{k=1}^s$.
5. If $\max\left(\frac{\|\mathbf{X}^{(l+1)} - \mathbf{X}^{(l)}\|_F}{\|\mathbf{X}^{(l)}\|_F}, \frac{|F(\mathbf{X}^{(l+1)}) - F(\mathbf{X}^{(l)})|}{F(\mathbf{X}^{(l)})}\right) \le \epsilon_{\mathrm{out}}$ and $l \ge \max(L_{\mathrm{BM}}) + \mathrm{length}(\boldsymbol{\theta})$, set $l := l + 1$ and **Break** outer loop.

End Outer loop and output $\mathbf{X} := \mathbf{X}^{(l)}$.

3. EXPERIMENTS

We conduct two types of experiments, i.e., filling missing blocks and randomly missing pixels. We compare the proposed method with two state-of-the-art solvers with similar principles: IDI-BM3D [9] (group-based sparsity under fixed transformed domain) and SAIST [8] (group-based low-rankness via spatially adaptive iterative SVT). We use peak signal-to-noise ratio (PSNR) and structured similarity index (SSIM) [22] to evaluate the results quantitatively. Both of them are higher for better results. All experiments are conducted under Windows 7 and Matlab R2015b (Version 8.6.0.267246) running on a desktop with an Intel(R) Core (TM) i7-6700 CPU at 3.40GHz and 16GB memory.

Missing blocks. We consider six 64×64 natural image patches each with a missing 16×16 central block, as in [8]. The parameter settings of our algorithm are as follows: patch size $w = 16$, number of patches in one group $n = 100$, search window of BM $n_{\mathrm{w}} = 50$, spatial step between two adjoining reference patches $n_{\mathrm{s}} = 4$, $c = 0$ in (4)[1], $\beta = 10$ in (7), $\boldsymbol{\theta} = (0, 0.3, 0.5, 0.7, 0.8)$ and $\eta = 0.25$ in (11), iteration set of updating grouping $L_{\mathrm{BM}} = \{1, 9, 17\}$, maximal iteration number of the DCA $l_{\max} = 100$ and ADMM $m_{\max} = 100$, tolerance of ADMM $\epsilon_{\mathrm{in}} = 1e{-}5$ and the DCA $\epsilon_{\mathrm{out}} = 5e{-}5$. For SAIST, we report the results from the paper. For IDI-BM3D, we test the authors' codes using a patch size 16×16 and default settings of other parameters.

The results by different methods are given in Fig. 2. We observe that IDI-BM3D fails to complete the texture in #3 and the edge in #4, whereas SAIST and our method yield reasonable inpainting results in all six cases. We also present the

[1] Although c should be positive to theoretically guarantee the convergence of the DCA, we find empirically that our algorithm still converges at $c = 0$.

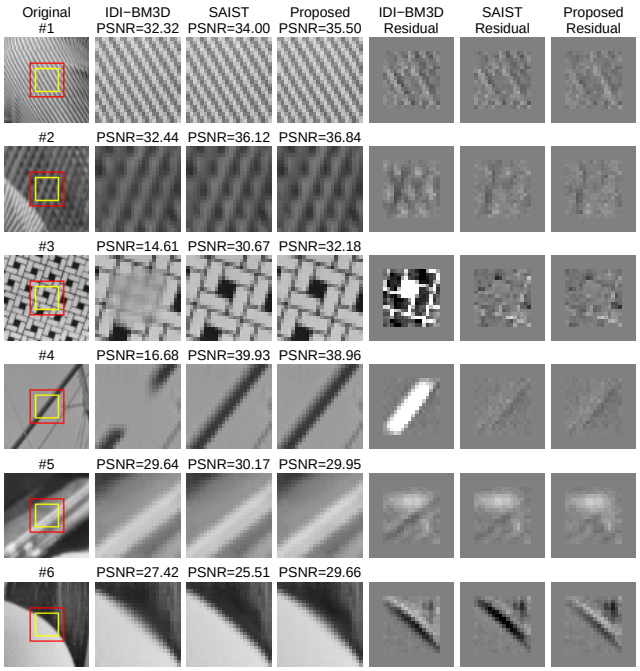

Fig. 2. Results of filling missing blocks. The missing regions are denoted by the small yellow squares and PSNR is calculated for those pixels only. For each method, we show both solutions and residuals (difference between the solution and the ground-truth). We zoom into the big red squares and scale the residuals by $\mathbf{X} \to 3\mathbf{X} + 0.5$ for better visualization.

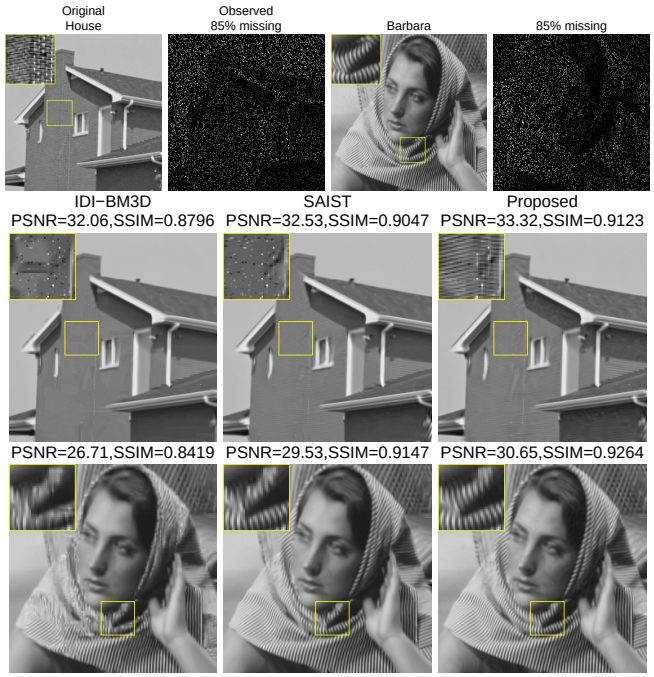

Fig. 3. Results of filling randomly missing pixels. All the zoomed-in regions of *House* undergo a same linear enhancement for better visualization.

residuals of each method (difference between the solution and the ground-truth), which highlight the image details removed by the algorithm. The results reveal that our residuals contain fewer noticeable structures than the other two methods. Quantitative evaluation suggests that our method achieves the highest PSNR values in four of six cases, while SAIST is the best in the other two cases. The average execution time of IDI-BM3D, SAIST, and our method is 1.28 min, 0.39 min, and 4.46 min, respectively.

Randomly missing pixels. We test two 256×256 natural images *House* and *Barbara* with 85% pixels randomly missing, shown in Fig. 3. The parameter settings of our algorithm are as follows: $w = 8$, $n = 60$, $n_{\rm w} = 20$, $n_{\rm s} = 4$, $c = 0$, $\beta = 10$, $\boldsymbol{\theta} = (0, 0.2, 0.4, 0.6, 0.7)$, $\eta = 0.25$, $L_{\rm BM} = \{1, 9, 17, 25, 33\}$, $l_{\max} = 100$, $m_{\max} = 100$, $\epsilon_{\rm in} = 1e-4$, and $\epsilon_{\rm out} = 5e-4$. For SAIST, we test the authors' codes using a maximal iteration number 600 and a noise variance 7.5. For IDI-BM3D, we test the authors' codes using a patch size 8×8. The other settings of the competing methods are left to their default ones.

The results by different methods are given in Fig. 3. We observe that IDI-BM3D is good at smooth regions, but not at textures. SAIST gives consistent results at various image features, but it is not as good as the proposed method in terms of fine detail preservation and overall visual quality. Regarding quantitative evaluation, our method achieves the highest PSNR and SSIM values for both testing images. The average execution time of IDI-BM3D, SAIST, and our method is 5.02 min, 6.91 min, and 27.57 min, respectively. Our method is time consuming because it requires inner ADMM iterations. A possible acceleration of our algorithm is to incorporate the recent proximal operator of l_{1-2} [23], which will be left to future research.

4. CONCLUSIONS

We have proposed a group-based low-rank model for image inpainting, in which an $l_{t,1-2}$ metric is incorporated to promote the low-rankness of each group. We have developed an efficient numerical scheme combined the DCA and ADMM for solving the proposed model, as well as an adaptive selection of the number of truncated singular values for each group. Numerical experiments have demonstrated that our method outperforms the state-of-the-art solvers in filling missing blocks and randomly missing pixels. Future works include accelerations of the proposed algorithm and extensions of $l_{t,1-2}$ to other image processing applications, such as [24, 25, 26].

5. REFERENCES

[1] M. Bertalmio, G. Sapiro, V. Caselles, and C. Ballester, "Image inpainting," in *Proc. 27th Annu. Conf. Comput. Graph. Interact. Techn.*, 2000, pp. 417–424.

[2] M. Bertalmío, A. L. Bertozzi, and G. Sapiro, "Navier-Stokes, fluid dynamics, and image and video inpainting," in *Proc. IEEE Conf. Comput. Vis. Pattern Recognit.*, 2001, pp. 355–362.

[3] J.-F. Cai, R. H. Chan, and Z. Shen, "A framelet-based image inpainting algorithm," *Appl. Comput. Harmon. Anal.*, vol. 24, no. 2, pp. 131–149, 2008.

[4] J. Mairal, M. Elad, and G. Sapiro, "Sparse representation for color image restoration," *IEEE Trans. Image Process.*, vol. 17, no. 1, pp. 53–69, Jan. 2008.

[5] A. A. Efros and T. K. Leung, "Texture synthesis by non-parametric sampling," in *Proc. IEEE Int. Conf. Comput. Vis.*, 1999, pp. 1033–1038.

[6] F. Cao, Y. Gousseau, S. Masnou, and P. Pérez, "Geometrically guided exemplar-based inpainting," *SIAM J. Imag. Sci.*, vol. 4, no. 4, pp. 1143–1179, 2011.

[7] C. Guillemot and O. Le Meur, "Image inpainting: Overview and recent advances," *IEEE Signal Process. Mag.*, vol. 31, no. 1, pp. 127–144, Jan. 2014.

[8] W. Dong, G. Shi, and X. Li, "Nonlocal image restoration with bilateral variance estimation: A low-rank approach," *IEEE Trans. Image Process.*, vol. 22, no. 2, pp. 700–711, Feb. 2013.

[9] F. Li and T. Zeng, "A universal variational framework for sparsity-based image inpainting," *IEEE Trans. Image Process.*, vol. 23, no. 10, pp. 4242–4254, Oct. 2014.

[10] E. Esser, Y. Lou, and J. Xin, "A method for finding structured sparse solutions to nonnegative least squares problems with applications," *SIAM J. Imag. Sci.*, vol. 6, no. 4, pp. 2010–2046, 2013.

[11] Y. Lou, P. Yin, Q. He, and J. Xin, "Computing sparse representation in a highly coherent dictionary based on difference of l_1 and l_2," *J. Sci. Comput.*, vol. 64, pp. 178–196, 2015.

[12] P. Yin, Y. Lou, Q. He, and J. Xin, "Minimization of l_{1-2} for compressed sensing," *SIAM J. Sci. Comput.*, vol. 37, no. 1, pp. A536–A563, 2015.

[13] Y. Lou, T. Zeng, S. Osher, and J. Xin, "A weighted difference of anisotropic and isotropic total variation model for image processing," *SIAM J. Imag. Sci.*, vol. 8, no. 3, pp. 1798–1823, 2015.

[14] P. Yin and J. Xin, "PhaseLiftOff: An accurate and stable phase retrieval method based on difference of trace and Frobenius norms," *Commun. Math. Sci.*, vol. 13, no. 4, pp. 1033–1049, 2015.

[15] Y. Lou, P. Yin, and J. Xin, "Point source super-resolution via non-convex L_1 based methods," *J. Sci. Comput.*, vol. 64, pp. 178–196, 2015.

[16] T.-H. Ma, Y. Lou, and T.-Z. Huang, "Truncated l_{1-2} models for sparse recovery and rank minimization," CAM Rep. 16-68, Univ. California, Los Angeles, 2016.

[17] T. Pham Dinh and H. A. Le Thi, "A D.C. optimization algorithm for solving the trust-region subproblem," *SIAM J. Optim.*, vol. 8, no. 2, pp. 476–505, 1998.

[18] D. Gabay and B. Mercier, "A dual algorithm for the solution of nonlinear variational problems via finite-element approximations," *Comput. Math. Appl.*, vol. 2, no. 1, pp. 17–40, 1976.

[19] K. Dabov, A. Foi, V. Katkovnik, and K. Egiazarian, "Image denoising by sparse 3-D transform-domain collaborative filtering," *IEEE Trans. Image Process.*, vol. 16, no. 8, pp. 2080–2095, Aug. 2007.

[20] J.-F. Cai, E. J. Candès, and Z. Shen, "A singular value thresholding algorithm for matrix completion," *SIAM J. Optim.*, vol. 20, no. 4, pp. 1956–1982, 2010.

[21] B. He and X. Yuan, "On the $O(1/n)$ convergence rate of the Douglas-Rachford alternating direction method," *SIAM J. Numer. Anal.*, vol. 50, no. 2, pp. 700–709, 2012.

[22] Z. Wang, A. C. Bovik, H. R. Sheikh, and E. P. Simoncelli, "Image quality assessment: From error visibility to structural similarity," *IEEE Trans. Image Process.*, vol. 13, no. 4, pp. 600–612, Apr. 2004.

[23] Y. Lou and M. Yan, "Fast L1-L2 minimization via a proximal operator," *arXiv preprint arXiv:1609.09530v4*, 2017.

[24] T.-H. Ma, T.-Z. Huang, and X.-L. Zhao, "Group-based image decomposition using 3-D cartoon and texture priors," *Inf. Sci.*, vol. 328, pp. 510–527, 2016.

[25] X.-L. Zhao, F. Wang, T.-Z. Huang, M. K. Ng, and R. J. Plemmons, "Deblurring and sparse unmixing for hyperspectral images," *IEEE Trans. Geosci. Remote Sens.*, vol. 51, no. 7, pp. 4045–4058, July 2013.

[26] X.-L. Zhao, F. Wang, and K. M. Ng, "A new convex optimization model for multiplicative noise and blur removal," *SIAM J. Imag. Sci.*, vol. 7, no. 1, pp. 456–475, 2014.